Wiley Analytical Science

The Current State of Reconstruction Technologies for 3D X-ray Microscopy including Algorithmic Innovation for AI-based Recovery

April 26, 10:00am - 11:00am EDT

Many properties can only be fully understood in 3D, such as porosity and tortuosity in porous materials, network connection maps in neuroscience, or mechanical properties in 3D additively manufactured structures. X-ray microscopy provides a unique method to image samples non-destructively in 3D across a wide range of materials and life sciences.

Watch this session during the WAS Virtual Conference:

Nicolas Guenichault, Ph.D.

Dr. Stephen T. Kelly, Ph.D.

Register Now

This talk is sponsored by ZEISS

ADVANCED FUNCTIONAL MATERIALS
www.afm-journal.de

Two-Photon Polymerization of Sugar Responsive 4D Microstructures

*Alexa Ennis, Deanna Nicdao, Srikanth Kolagatla, Luke Dowling, Yekaterina Tskhe, Alex J. Thompson, Daniel Trimble, Colm Delaney, and Larisa Florea**

Stimuli-responsive hydrogels have attracted much attention owing to the versatility of their programmed response in offering intelligent solutions for biomimicry applications, such as soft robotics, tissue engineering, and drug delivery. To achieve the complexity of biomimetic structures, two photon polymerization (2PP) has provided a means of fabricating intricate 3D structures from stimuli-responsive hydrogels. Rapid swelling hydrogel microstructures are advantageous for osmotically driven stimuli-response, where actuation speed, that is reliant on the diffusion of analytes or bioanalytes, can be optimized. Herein, the flexibility of 2PP is exploited to showcase a novel sugar-responsive, phenylboronic acid-based photoresist. This offers a remarkable solution for achieving fast response hydrogel systems that have been often hindered by the volume-dependent diffusion times of analytes to receptor sites. A phenylboronic acid-based photoresist compatible with 2PP is presented to fabricate stimuli-responsive microstructures with accelerated response times. Moreover, microstructures with programmable actuation (i.e., bending and opening) are fabricated using the same photoresist within a one-step fabrication process. By combining the flexibility of 2PP with an easily adaptable photoresist, an accessible fabrication method is showcased for sophisticated and chemo-responsive 3D hydrogel actuators.

1. Introduction

Hydrogels have epitomized smart materials due to their ability to respond to external stimuli by converting it into other forms of energy. Through the integration of such stimuli-response, their application has spanned biofabrication,[1] additive manufacturing,[2] and even soft robotics.[3] Liu et al. categorized stimuli-responsive hydrogel actuators into three types: a) hydrogel matrices embedded with active elements (e.g. magnetic particles or free ions) which respond to external fields (e.g. magnetic or electric fields); b) hydrogel structures with cavities driven by hydraulic or pneumatic pressures; and c) stimuli-responsive hydrogels actuated by changes in osmotic pressure.[4]

Of particular interest to this work are stimuli-responsive hydrogels that undergo changes in volume as a result of osmotic pressure, leading to the diffusion of water in and out of the hydrogel network. To this end, stimuli-responsive networks have provided opportunity to detect and respond to external stimuli such as biomolecules,[5] water,[2a] temperature,[6] light,[3a] and pH,[7] among others. However, the main drawback of osmotically driven hydrogel actuators is their low actuation speed, where actuation force and response time are inextricably linked. This represents one of the major challenges for stimuli-responsive hydrogels which rely on the diffusion of analytes or bioanalytes. A pertinent example can be seen in the use of phenylboronic acids (PBAs) as promising candidates for the realization of sugar-responsive (D-fructose, D-galactose, D-mannose, and D-glucose) hydrogels.[8] In the presence of 1,2- and 1,3-diols in aqueous media, PBAs yield a boronate ester.[9] When immobilized in a hydrogel network, this can be used to generate a physical response, either through repulsion of the negatively

A. Ennis, D. Nicdao, S. Kolagatla, Y. Tskhe, C. Delaney, L. Florea
School of Chemistry & AMBER
The SFI Research Centre for Advanced Materials and BioEngineering Research
Trinity College Dublin
Dublin 2 D02 PN40, Ireland
E-mail: floreal@tcd.ie

The ORCID identification number(s) for the author(s) of this article can be found under https://doi.org/10.1002/adfm.202213947.

DOI: 10.1002/adfm.202213947

L. Dowling, D. Trimble
Department of Mechanical & Manufacturing Engineering
Trinity College Dublin
Dublin 2 D02 PN40, Ireland

A. J. Thompson
Department of Surgery & Cancer
Queen Elizabeth the Queen Mother Wing
St Mary's Hospital
Imperial College London
South Wharf Road, London W2 1NY, UK

A. J. Thompson
The Hamlyn Centre
Institute of Global Health Innovation (IGHI)
Imperial College London
Exhibition Road, South Kensington, London SW7 2AZ, UK

charged boronate esters[10] that leads to the expansion of the hydrogel network or a shrinking[11] actuation caused by linkage of two boronic acids with a single sugar molecule that acts as an additional crosslinking point.[12] To date, PBA-functionalized hydrogels have primarily been explored on the macro-scale, exhibiting response times to reach equilibrium swelling typically in the order of minutes to hours.[8a,c,13] As response rate is generally dependent on the square of the hydrogel's characteristic dimensions,[13c] the reduction of hydrogel size to a micron regime can yield a profoundly accelerated response time.[8a,14]

Direct laser writing by two photon polymerization (2PP) has been recently explored as a 3D fabrication technology of choice for the generation of soft micro-machines, offering the exciting opportunity of translating the extensive library of macro-scale stimuli-responsive hydrogels to the micron (and even submicron) scale. Examples of stimuli-responsive structures produced by 2PP include: 1) magnetic micro-swimmers (realized by post-fabrication coating with metals such as Ni[15] or incorporation of Fe_3O_4 nanoparticles[16]) actuated by rotating magnetic fields; 2) microstructures fabricated in liquid crystal elastomeric (LCEs) networks, capable of thermo-,[17] or photo-actuation,[18] and 3) a limited number of stimuli-responsive hydrogel actuators based on poly(N-isopropylacrylamide) copolymers or poly(ionic liquids), sensitive to temperature,[19] solvent[20] or changing pH conditions.[7,21]

Not only is 2PP one of the few technologies compatible with hydrogel fabrication at the micro-scale, but it also enables the realization of sophisticated 3D (including high-aspect ratio) microstructures that can undergo anisotropic and programmable shape change. Remarkably, this can be achieved in one fabrication step, with a single material, at atmospheric temperature and pressure. This dramatically simplifies fabrication protocols. The transition from isotropic (e.g. via UV lithography) to anisotropic response (via 2PP), offers unsurpassed control in 3D hydrogels at the micro-scale and is enabled by accessible programming of writing parameters, such as laser power, writing speed, hatching, and slicing distances or direction. Dynamic variation of these parameters enables the realization of domains within the polymer network of controlled stiffnesses, mechanical properties, and by extension, controlled expansion upon introduction of the desired stimulus. For example, increased distances in vertical slicing or lateral hatching, result in a less-compact network, capable of increased water uptake. Similarly, precise control of laser dosage in 3D (via controlled laser power and writing speed), enables domains with different degrees of polymerization or cross-linking, which possess distinctive abilities to actuate. These capabilities have been explored, to date, for the generation of a bilayered hydrogel constructions capable of unidirectional bending[19a] or opening/closing,[21g] realization of hinge-type assemblies,[7,21a] and even shape-changing origami type structures.[22] Such fine control of the polymer network in 3D brings significant possibilities in functionality that have remained untapped hitherto. It would, therefore, be highly advantageous to translate the vast library of functional hydrogel actuators, from the macro- to the micro-scale. However, this is not straight-forward. As highlighted in a recent review on state-of-the-art materials for 2PP, despite the wide range of potential functional monomers available, the realization of stimuli-responsive hydrogel photoresists requires careful photoresist optimization, with precise control of solution composition, viscosity, stability, and optical properties.[23]

Several challenges arise when attempting to meet such photoresist standards for 2PP. As 2PP takes place on a voxel-by-voxel basis, it demands rapid curing in the confined laser spot, which often necessitates low-solvent content in the photoresist (the majority of commercially available photoresists are solvent-free) and high concentration of cross-linkers, in particular cross-linkers with multiple unsaturated bonds. Such requirements are not conducive to hydrogel fabrication at the macro-scale, where high solvent-content and low cross-linker concentration (<2 mol%) are preferred. Additionally, volatile organic solvents, commonly used at the macro-scale to dissolve monomers, cross-linkers, and photoinitiators, are prone to evaporation during the 2PP process. This results in the generation of micro-explosions during the laser writing process that can impede the resolution of the final 3D structure. Measures including incorporation of high boiling-point organic solvents, such as ethylene glycol[19a] and ethyl lactate,[7,21g] to improve photoresist stability during 2PP, require optimization on a case-by-case basis. Solvent choice must clearly be improved to produce more versatile hydrogel photoresists for 2PP.

Herein, we propose a novel photoresist for the generation of sugar-responsive hydrogel microstructures based on a phenylboronic acid copolymer (**Figure 1**, Figure S1, Supporting Information). Through introduction of an ionic liquid (IL), namely tetrabutylphosphonium chloride ($[P_{4,4,4,4}][Cl]$), as the water-miscible solvent for our PBA-containing photoresist formulation, we achieve excellent solubilization of all desired components; (3-(acrylamido)phenylboronic acid (Am-PBA), acrylamide (Am), 7-diethylamino-3-thenoylcoumarin (DEATC), and the necessary inclusion of relatively small percentage (5 mol.%) of a bifunctional cross-linker, N,N-Methylenebisacrylamide (MBIS), to facilitate high swelling capabilities in the resulting hydrogel structures (height increase of up to 234.5% ± 1% from dry to hydrated in 5 mM fructose solution). Directional actuation of the 2PP-fabricated microstructures (e.g. beams, flower-like structures) was achieved by introducing inhomogeneous cross-linking via varied laser dosages, to create regions with different degrees of swelling. These microstructures possess remarkable structural integrity and reversible mobility when exposed to aqueous flow and show rapid (equilibrium swelling is reached within a few s) and reversible actuation in response to fructose solutions. The example presented herein showcases a robust chemo-responsive hydrogel formulation that can be easily adapted for a wide range of other chemically responsive hydrogel systems.

2. Results and Discussion

2.1. 2PP of Sugar-Responsive Microstructures

The monomers, (3-(acrylamido)phenylboronic acid (Am-PBA) and acrylamide (Am), the photoinitiator, 7-Diethylamino-3-thenoylcoumarin (DEATC), and the cross-linker, N,N-Methylenebisacrylamide (MBIS) were all dissolved in the IL solvent, tetrabutylphosphonium chloride ($[P_{4,4,4,4}][Cl]$). All components were solubilized under ambient conditions. This is owed to the

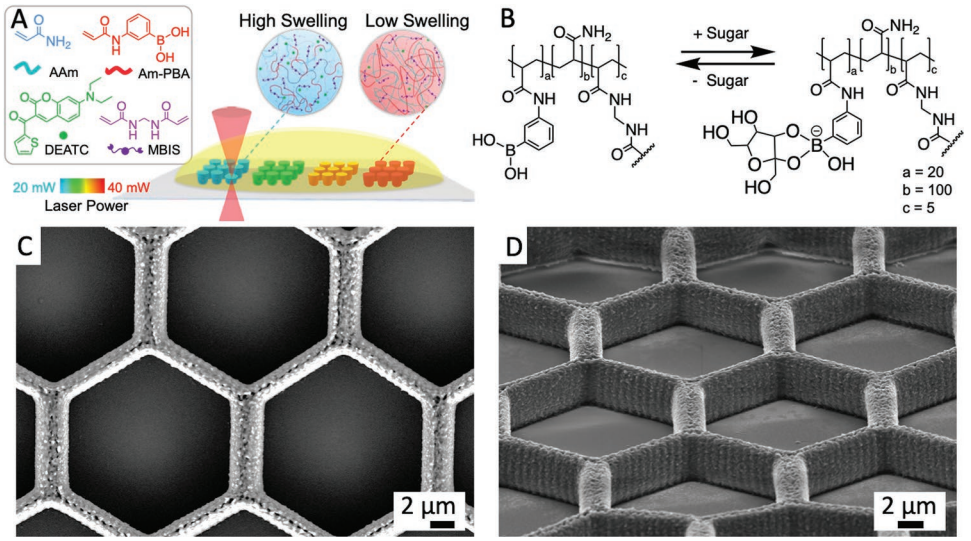

Figure 1. Two-photon polymerization of sugar-responsive hydrogel microstructures. A) Chemical structures of photoresist components, acrylamide (Am), 3-(acrylamido)phenylboronic acid (Am-PBA), 7-diethylamino-3-thenoylcoumarin (DEATC), and N,N-Methylenebisacrylamide (MBIS) and schematic of the fabrication process of arrays of micro-pillars using different laser powers; B) Scheme showing the reaction between the boronic acid polymer and sugar molecules in PBS buffer conditions, showing the change in charge on the boron center; C,D) SEM image of a honeycomb structure fabricated at 20 mW and 5 mm s^{-1}, top down and taken at a 60° tilt, respectively.

presence of a polar anion and relatively non-polar cation in the IL solvent that enables the dissolution of a range of polar and non-polar components.

To initiate radical polymerization of the precursor solution, the near-IR femtosecond LASER excites the photoinitiator, DEATC, to produce initiator radicals. The 2PP writing process continues as monomeric units (Am-PBA and Am) reacting via radical polymerization of the acrylate groups to form polymeric chains. Simultaneously, a network is formed between the propagating chains of poly(Am-PBA-co-Am) with the cross-linker, MBIS (Figure 1A,B). Polymerization occurs on a voxel-by-voxel basis. Fabricated microstructures were found to have a spatial resolution of less than a micron, as shown through the fabrication of single voxel width lines at different laser powers (Figure S2, Supporting Information), where line widths of <400 nm were achieved at the lowest laser dosage used (15 mW 20 000 µm s^{-1}). A laser power range between 20 and 40 mW was determined for successful micro-fabrication of the structures. This is a comparable range (≈20 mW difference) with other resists used in 2PP. For example, Hippler et al. used a range between 30 mW (60%) and 37.5 mW (75%) and a writing speed of 1 mm s^{-1} for their thermo-responsive photoresist that incorporated poly(*N*-isopropylacrylamide) (pNIPAAM).[19a] Meanwhile, Duan and co-workers showcased pH-responsive microstructures with a p(acrylic acid-*co*-NIPAM) resist using laser powers of 12 mW (24%)–40 mW (80%) and a scan speed of 8–25 mm s^{-1}.[7] Our microstructures revealed an expansion of up to ≈165.2% (±1.6%, $n \geq 11$) in area from dry to full expansion in 25 mM fructose. This high swelling capability is attributed to the presence of the two-arm cross-linker (MBIS) in a relatively small proportion (5 mol.%) and the presence of a high content of the IL solvent (≈50 wt.%) in the photoresist. Previous studies have shown that in the case where photo-induced free radical polymerization of methyl methacrylate was carried out in an IL (1-butyl-3-methylimidazolium hexafluorophosphate), the rate constant of polymerization can be considerably increased. This is owed to the high charge density of the IL that lowers the activation energy of propagation via a charge transfer interaction. The chain termination rate also decreases due to the viscosity of the IL.[24] This allows for a broader range of writing parameters to be used while retaining the hydrogel's high swelling capability.

The hydrogel microstructures presented herein exhibited a rapid response to fructose due to the immobilized PBA moieties within the hydrogel network that yield a boronate ester when exposed to 1,2- or 1,3-diols (e.g., sugars) in aqueous media.[9] Consequently, once exposed to fructose solutions, repulsion between negatively charged boronate esters lead to an expansion (swelling) of the network (**Figure 2**A). This behavior is also supported by the change in hydrophilicity of bulk films fabricated from the PBA-based material, where a contact angle of 27.6 + 2.9° ($n = 9$) was obtained for films hydrated in 100 mM fructose solution, compared to 91.1 + 4.5° ($n = 9$) when the films were exposed to PBS only. This indicates that the material becomes much more hydrophilic upon sugar binding. To characterize swelling behavior, the same writing parameters were implemented into a 4 × 4 array of pillar structures 20 µm in diameter and 30 µm in height. The pillars were imaged from above, using an upright epifluorescence microscope, and the 2D area was measured using ImageJ. The areas of pillars was compared for a range of fructose concentrations (Figure 2B; Video S1, Supporting Information), in which swelling properties can be tuned by the laser dosage used during structure fabrication. Pillar areas steadily increased with increasing fructose concentrations for all groups, and for the lowest laser dosage condition (20 mW) equilibrium swelling was reached in ~90 s when exposed to 5 mM fructose solution (Figure S3, Supporting Information). This is considerably faster than bulk

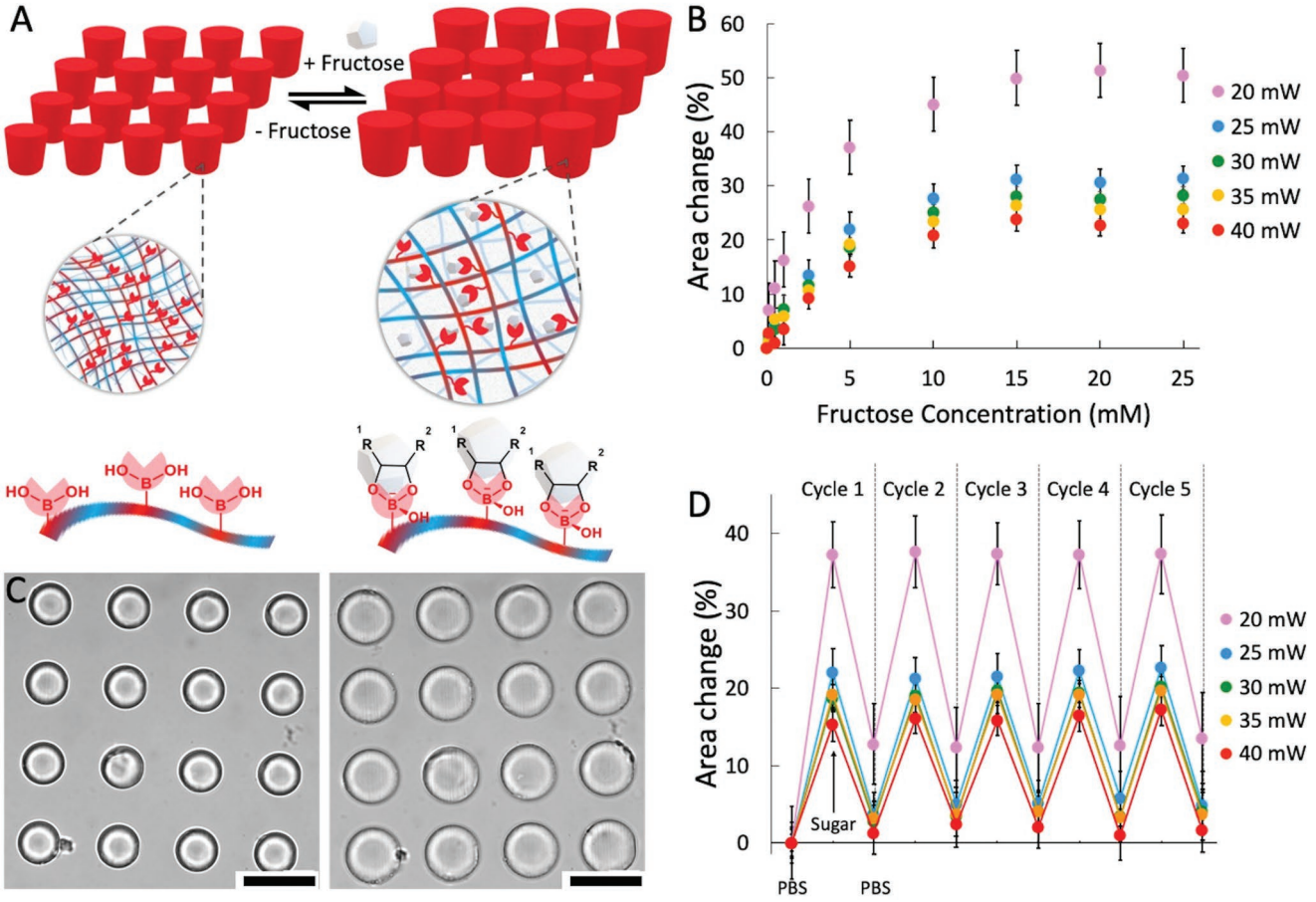

Figure 2. Swelling capability of the boronic acid hydrogel. A) Diagram showing mechanism of hydrogel swelling; B) Graph of the increase in area of the top of pillars ($n \geq 11$) with a designed diameter of 20 μm and a height of 30 μm, fabricated at different laser powers (20–40 mW), as the concentration of fructose increases from 0 mM (PBS) to 25 mM; C) Bright field microscopy images showing the increase in size of pillars fabricated 20 mW and 10 mm s^{-1} when the hydration solution changes from PBS (left) to 25 mM fructose in PBS (right); D) Graph showing that the reproducibility of actuation during cycles of PBS and fructose solution (5 mM) in PBS, at all laser powers employed for structure fabrication (20–40 mW). Scale bar represents 50 μm in (C).

hydrogel boronic acid materials that take from 30 min to several hours to reach equilibrium.[8a,13b,25] The increase in speed of actuation can be directly attributed to the miniaturization of structures that counteracts the slow diffusion of diol species into the hydrogel matrix. From PBS to 25 mM fructose, the largest expansion observed was for the lowest laser dosage condition (20 mW) with an increase in area of ~50.5% (±4.2%, $n \geq 11$). The highest laser dosage condition (40 mW) showed an increase in area of ~23.2% (±1.8%, $n \geq 11$). The same trend was observed for each of the fructose concentrations studied (Figure 2B). It has been previously demonstrated that increasing laser dosage (i.e., via an increase in laser power) increases the cross-linking density of the network, therefore limiting its expansion.[7,19a] In contrast, structures fabricated at lower laser powers are less densely cross-linked and have a greater ability to swell. The swelling behavior in response to glucose was also examined, and it was found that while the same trend was followed (the microstructures increase in size as the concentration of glucose is increased), the swelling response to glucose was much lower than that observed for fructose (Figure S4, Supporting Information). This is due to higher binding constant of fructose with the acrylamido phenyl boronic acid in comparison to glucose. The boronic acid preferentially binds to the 5-membered ring form of sugars that have syn-periplanar hydroxyl groups available for binding to the boronic acid.[26] The β-D-fructofuranose form of fructose makes up 25% of the total composition of fructose in D_2O at 31 °C[27] while the α-D-glucofuranose form of glucose that has syn-periplanar hydroxy groups available for bonding only makes up 0.14% of the glucose available.[28] Figure S4 (Supporting Information) shows the response of 5 arrays of pillars fabricated at the same laser dosages used above, in response to increasing concentrations of glucose (1, 10, 25, 50, 75, 100, 150, 200, 300, and 400 mM).

To ensure a reliable and defined actuation is occurring, the sugar response of all micro-pillars was tested over 5 hydration cycles in PBS and 5 mM fructose solution, respectively (Figure 2C,D). After repeated cycles, it is clearly shown that the pillars fabricated at 20 mW have the highest degree of swelling when exposed to PBS and fructose solutions, and that all pillars show reversible and reproducible actuation.

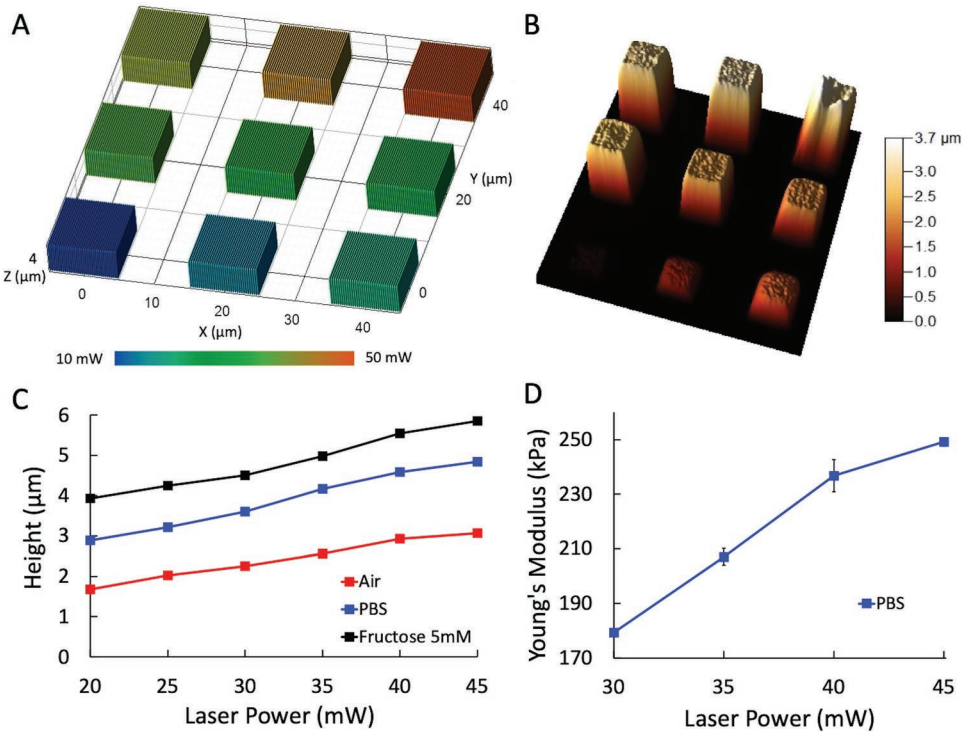

Figure 3. Height profiles and Young's modulus measurements of the micro-cubes. A) Design of the array of 10 μm × 10 μm × 4 μm cubes fabricated at different laser powers (10–50 mW) used for all AFM measurements; B) 3D height plot of the micro-cube array fabricated at 10–50 mW in the dry state; C) Graph showing height of cubes at each laser power, in the dry state, PBS, and fructose 5 mM. D) Graph showing Young's modulus of micro-cubes fabricated at different laser power upon hydration in PBS.

The swelling and mechanical properties of the micro-structures were also investigated using atomic force microscopy (AFM). An array of cuboidal structures 10 μm × 10 μm × 4 μm were fabricated with laser powers from 10 mW (20% maximum laser power) to 50 mW (100%) with a 5 mW (10%) step (**Figure 3**A,B). AFM topography in air shows that at 90% laser power the height of the cube after washing and drying is 3.06 ± 0.02 μm, which is a ~25% decrease in height from the designed 4 μm. The AFM height images in PBS buffer show a significant increase in the height of the structures from the dry state (Figure 3C; Figures S5 and S6, Supporting Information), where the percentage increase in height ranges from 57% to 72% (±2.1%, $n = 3$) as the laser power is decreased from 40 to 20 mW (Figure S5, Supporting Information). The height of the cubes is further increased when the liquid medium is changed to fructose solution (5 mM). Here, we observed an additional ~21.0% (±1.2%, $n = 3$) to ~36.0% (±1.1%, $n = 3$) height increase from PBS to fructose (5 mM) when laser powers of 40 and 20 mW were used (Figure 3C). The overall percentage height increase of the micro-cubes from air to fructose (5 mM) was found to be in the range of 89.5% (±1.3%, $n = 3$)–134.5% (±1.0%, $n = 3$) when the laser power was decreased from 40 to 20 mW (Figure S5, Supporting Information). Young's modulus measurements were also performed on the micro-cubes using atomic force microscopy, where the Young's modulus values in air for 30–45 mW (60–90%) laser powers are in the 1.47 (±0.05; $n = 3$)–1.55 (±0.03; $n = 3$) GPa range, with an increasing trend from lower to higher laser power. When the medium is changed to PBS, the cubes hydrate as described above, becoming much softer, with Young's modulus values in PBS in the range of 179.3 (±1, $n = 3$)–249.2 (±1.5) kPa for laser power of 30–45 mW (Figure 3D). The AFM results show that the fabricated structures hydrate in PBS and fructose solutions, with a considerable reduction in Young's modulus. For example, micro-cubes fabricated at 30 mW, show a reduction in Young's modulus from 1.47 (±0.05; $n = 3$) GPa to 179.3 (±1, $n = 3$) kPa upon hydration in PBS, of almost 4 orders of magnitude.

To demonstrate that thesesoft micro-structures maintain their shape integrity during hydration (PBS and fructose solutions) and even active flow, complex twisted vase microstructures (23 μm in height and 32 μm in diameter) with a small diameter base (6.6 μm in diameter) were fabricated (**Figure 4**). These twisted vases are composed of a single laser dosage and are anchored to the slide with unsupported overhang features. Open structures such as these are a current challenge for hydrogel resists as such structures are subject to collapse due to the intrinsic softness of hydrogels. The vases fabricated herein remained upright after expansion in PBS and when exposed to 100 mM fructose solutions and can reversibly shrink in PBS (Figure S8 and Video S2, Supporting Information). Notably, they also demonstrated mechanical stability under an active flow (Video S3, Supporting Information).

To implement directionality in actuation, we exploited the flexibility of laser control in 2PP to create bilayer structures – a typical approach in soft robotics where domains of stiffness are altered based on cross-linking density of the hydrogel network. We designed a bi-layer blooming flower structure, in which each layer is fabricated at a different laser dosage, to

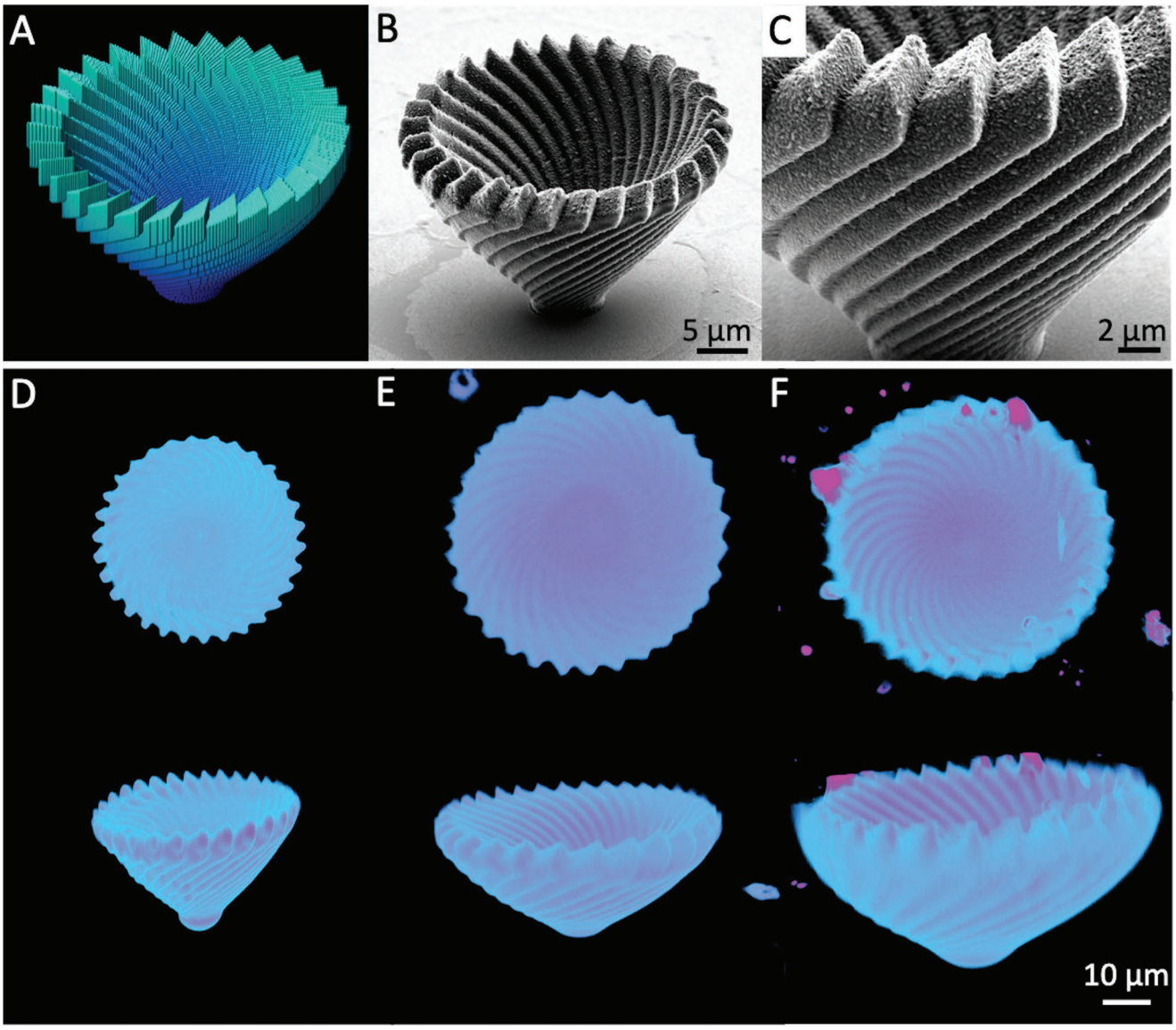

Figure 4. Complex 3D soft hydrogel vase structure. A) Design of twisted vase structure of 23 µm in height, with a top diameter of 32 µm and a base diameter of 6.6 µm; B) SEM image and C) SEM detail of the vase structure fabricated at a laser power of 25 mW and 10 mm s^{-1}. D–F) confocal microscopy images showing top-down view and side profile of the 3D vase in the dry state, hydrated in PBS and in 100 mM fructose solution, respectively.

demonstrate directed actuation with our photoresist (Video S6 and Figure S9, Supporting Information). By utilizing the inner (20 mW) and outer layers (30 mW), a blooming actuation (i.e., opening of flower) was seen when the hydration solution was changed from PBS to 100 mM fructose. One setback seen with this design is the limited reversible actuation (i.e., closing of flower). Here, the challenge of working solely with intrinsically soft materials is shown as the network is too soft to lift the petals back to their original position. Although the actuation may be limited in the Z-plane, a second design demonstrating directed actuation along the XY plane was achieved (**Figure 5**). Here, a bi-layer beam design with a length of 40 µm has shown an average deformation of 16.6° ± 0.30° when exposed to fructose. One side of the beam was fabricated at 20 mW and the other side was fabricated at a laser power of 25 mW. These parameters were chosen as they gave the largest difference in swelling capacity between two successive laser powers (5 mW difference). SEM imaging (Figure 5B,C) confirmed good attachment between the two sides of the beam. After polymerization and development, in the dry state, the beam is at an average angle of 70.0° ± 0.14° to the base. This initial bend toward the side fabricated at the lower laser power (20 mW) is due to the difference in width between the two sides caused by the fabrication parameters. Upon hydration in PBS, the beam bends further toward the side fabricated at lower laser power reaching an angle of ~48.2° to the base (Figure 5D; Video S4, Supporting Information). Upon the addition of fructose, the beam straightens to a 75.3° ± 0.21° angle to the base (Figure 5E; Video S5, Supporting Information). This is in agreement with the FEA simulations shown in Figure 5G,H for the beam, based

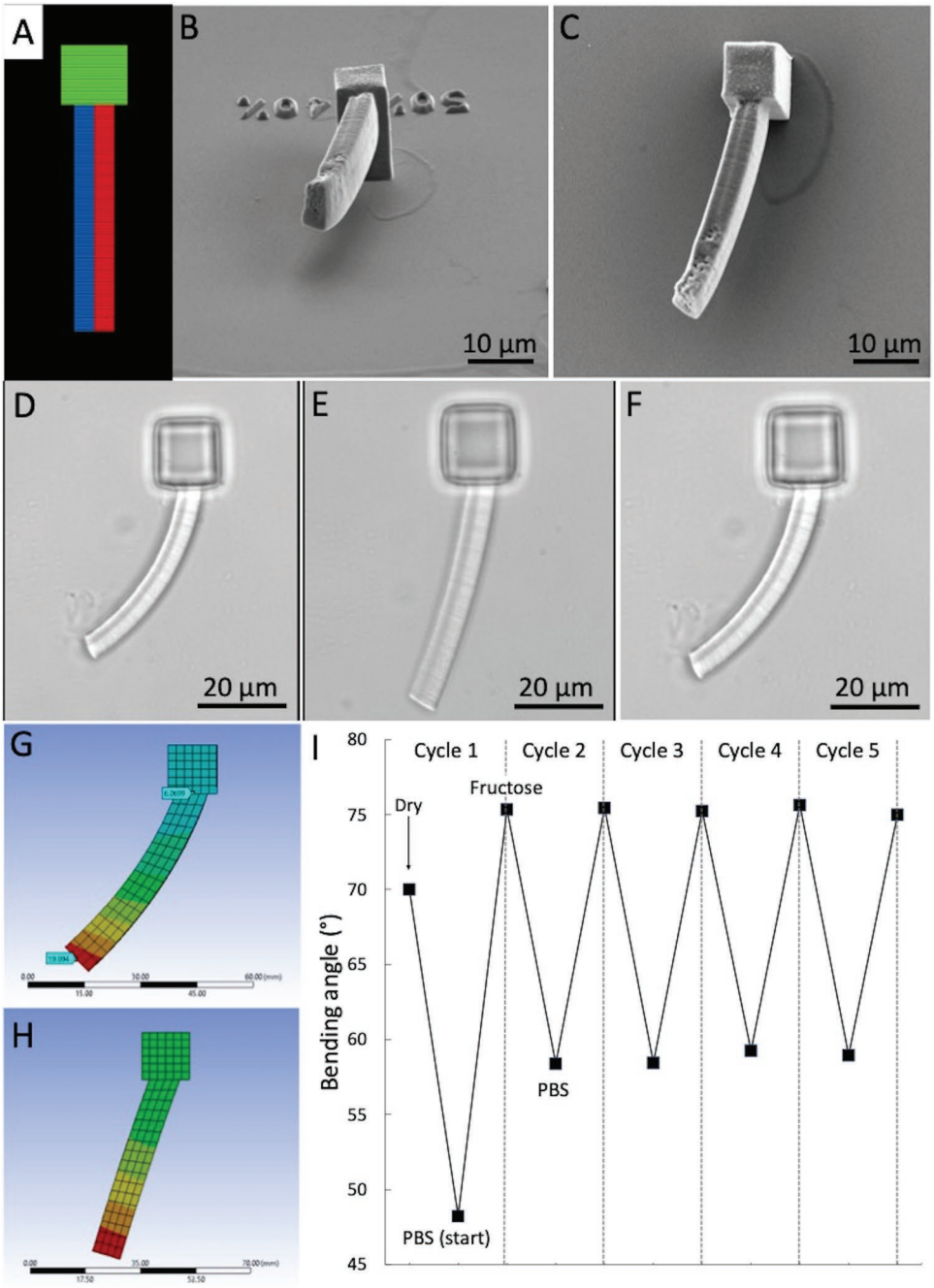

Figure 5. Responsive bilayer beams. A) Design of the bilayer beam, red denotes volume fabricated at 25 mW laser power, blue denotes volume fabricated 20 mW laser power and green denotes the base of the beam fabricated at 30 mW; B) SEM image of beam structure at 60°; C) Top down SEM image of beam structure; Optical microscope image of D) Beam bending while hydrated in PBS; E) Beam straightening while in 5 mM fructose solution; F) Beam bending when the hydration media is reverted to PBS; FEA models of beam in G) PBS solution and H) 5 mM fructose; I) graph showing the bending angle of the beam through multiple PBS to 5 mM fructose cycles.

on the properties of the bilayer materials. After the addition of fructose, the beam returned to an angle of 58.4° ± 0.14° when reimmersed in PBS, a difference of ≈10.2° ± 0. 1° compared to the previous bending angle observed in PBS (Figure 5F). However, after this initial cycle no further loss to the degree of actuation is observed and the actuation of the beam is reproducible over the remaining 4 cycles (Figure 5I). The bending angle of the beam in PBS at the start of the experiment compared to subsequent cycles is likely due to incomplete removal of fructose from the structure during the first washing step (a certain concentration of PBA remains in the bound form). The degree of actuation of the beam could be further improved by reducing the width of the beam, increasing the aspect ratio, or combining the PBA-based layer with a secondary non-responsive

polymer material. To further explore this, we designed a dual-material gripper microstructure (Figure S10, Supporting Information), achieved through sequential fabrication steps, that enables the incorporation of areas of the PBA-based hydrogel to serve as pistons to direct the bending of two flexible arms (1 μm thin, 10 μm long) fabricated in the commercial IP-L 780 photoresist (Nanoscribe GmbH). The gripper mechanism lies flat with dimensions of 12 μm × 30 μm and comprises an outer frame, two suspended thin arms (1 μm) which are buttressed by the PBA-based hydrogel that is incorporated in a second fabrication step. After fabrication and development, the structures bear good fidelity to the design (with the arms separated by 3.5 μm). Upon hydration in PBS buffered solution, swelling of the soft hydrogel straightens the pendant arms. Upon exposure to fructose 100 mM (5 min), the arms are seen to meet and close. While this is a proof-of-concept application, it serves to demonstrate the potential for multi-material fabrication where soft responsive hydrogels, like the ones described herein, can drive the actuation of thin, flexible components made of inert polymers. We believe that this is the key in order to create responsive micro-robotic structures capable of sustained and reversible actuation.

3. Conclusion

A novel stimuli-responsive hydrogel-based photoresist capable of fabricating microstructures via 2PP has been shown in this paper. The swelling properties in a range of fructose concentrations (0–25 mM) were characterized across a range of laser dosages. It was found that with increased laser exposure comes reduced actuation. This trend in actuation based on laser dosage was also shown to be reversible, over several cycles, with no sign of fatigue. To demonstrate the value of a stimuli-responsive resist for 2PP, complex, 3D-twisted vases were fabricated. The vases demonstrated reversible actuation (expansion and shrinkage) between fructose and PBS environments, respectively. More notably, the vases were able to withhold stature under a flow showcasing their mechanical stability. For the next step, directed actuation was explored through sophisticated 3D structures; bio-inspired blooming flowers and bending bilayered beams. It was seen in both designs that controlling laser dosage harnesses control over actuation response that can be exploited to create sophisticated, stimuli-responsive micromachines for applications, such as continuous glucose monitoring and dual-material microgrippers. This photoresist expands the limited library of stimuli-responsive hydrogels for 2PP and extends the opportunity to use this controllable and robust fabrication method to create stimuli-responsive microstructures with desirably directed and rapid actuation.

4. Experimental Section

Materials and Reagents: 3-(acrylamido)phenylboronic acid (98%), acrylamide 98%, N,N-Methylenebisacrylamide 99% (MBIS), were acquired from Sigma–Aldrich, Ireland, and used as received. Tetrabutyl phosphonium chloride ([$P_{4,4,4,4}$][Cl]), 80% in water was obtained from TCI, Japan. The photo-initiator, 7-Diethylamino-3-thenoylcoumarin (DEATC), was obtained from Alpha chemical, USA. All other solvents, including acetone, 2-propanol, ethanol, and methanol were HPLC grade, purchased from Sigma–Aldrich, Ireland, and used without further purification. Propylene glycol methyl ether acetate (PGMEA) was also purchased from Sigma–Aldrich, Ireland, and used without further purification.

Table 1. Photoresist 1 components.

Compound	Molecular weight [g/mol]	Moles [mmol]	Mass [mg]	Ratio [mol%]
acrylamide	71.08	4.22	300.0	100
3-acrylamidophenylboronic acid	190.99	0.84	161.2	20
N,N'-methylenebisacrylamide	154.17	0.21	32.5	5
tetrabutylphosphonium chloride	294.88	1.70	500.0	40
7-diethylamino-3-thenoylcoumarin	327.4	0.04	13.8	1

Photoresist Preparation: The monomer mixture consisted of acrylamide, 3-(acrylamido)phenylboronic acid (20 mol.% to acrylamide), MBIS cross-linker (5 mol.% to acrylamide) and DEATC (1 mol.% to acrylamide). All components were dissolved in the IL solvent ($P_{4,4,4,4}$Cl) at a 3:5 wt.% of acrylamide to IL. This photoresist was used for the fabrication of all micro-structures shown in this work (Photoresist 1, **Table 1**).

In order to explore further the suitability of such photoresist for 2PP fabrication, additional photoresists of increasing IL content (from 40 to 150 mol.% in relation to acrylamide) were also investigated, while keeping the other components constant (Tables S1 and S2, Supporting Information). It was found that successful fabrication was still possible, even at >70 wt.% IL in the photoresist, indicating the great degree of freedom in terms of photoresist composition. In comparison, successful fabrication was not achieved in the current experimental conditions, when the IL was replaced with other common organic solvents (tetrahydrofuran, dimethylsulfoxide, ethyl lactate) at the same weight content as shown for Photoresist 1 (Table 1).

Direct Laser Writing Fabrication: A commercial DLW workstation, Photonic Professional Nanoscribe GmbH, was used for the fabrication of the 3D structures via two-photon polymerization using the photoresist indicated in Table 1. The system operates at a wavelength of 780 nm, using a 170 mW femtosecond solid–state laser that delivers 120 fs pulses with an 80 MHz ± 1 MHz repetition rate. An oil-immersion configuration was employed, using a 63× immersion objective (NA = 1.4, WD = 190 μm) (Zeiss, Plan Apochromat). Sample positioning was controlled by a 3D galvo translation stage.

To ensure attachment of the 3D microstructures to the substrate, all glass substrates (high precision round cover slips, 30 mm, thickness 170 ± 5 μm; No 1.5; acquired from Gerhard Menzel GMBH) underwent silanization treatment. First, the slides were cleaned with acetone, isopropanol, ethanol, methanol, and DI water; followed by UV Ozone for 20 min (Osssila, United Kingdom). Slides were then submerged in a solution of 3-(trimethoxysilyl)propyl methacrylate (Sigma–Aldrich; 3 vol.% in ethanol with 0.1 vol.% Acetic acid) for 1 h. The slides were removed from this solution and rinsed with ethanol, dried under nitrogen, and baked in an oven at 60 °C for 3 h.

To begin the fabrication process, a single drop of the photoresist was placed on the center of the silanized surface. A drop of oil (Zeiss Immersol 518F) was placed in the center of the opposite side. The scan speed for all structures was kept constant at 10 mm s^{-1} while the laser power was varied between 15 and 45 mW. Once the fabrication process was complete, structures were carefully developed in propylene glycol methyl ether acetate (PGMEA) to remove residual unpolymerized photoresist.

For the fabrication of the proof-of-concept micro-gripper (Figure S10, Supporting Information), a two-step procedure was implemented, where the fabrication of both materials, namely IP-L 780 commercial photoresist (1st step) and PBA-based hydrogel (Photoresist 1) was performed sequentially in the oil-immersion configuration using a 63×

objective (NA = 1.4, WD = 190 µm) (Zeiss, Plan Apochromat). The 3D structure was designed in Blender and then converted into DeScribe software as suitable for fabrication on the Nanoscribe GmbH system. A slicing distance of 0.2 µm, hatching of 0.2 µm, and no contour lines were applied for the entire structure. To precisely fit the responsive polymer blocks between the moving arms of micro-gripper and the main frame attached to the surface, marker alignment was used. A laser power of 20 mW was used to fabricate the IP-L 780 part of micro-grippers (Figure S10, Supporting Information, represented in purple). After this, the structure was developed in PGMEA for 20 min followed by IPA for 3 min. For the second step, the PBA-based photoresist (Photoresist 1) was used and a laser power of 35 mW was employed for fabrication (Figure S10, Supporting Information, represented in green). A scanning speed of 10 mm s^{-1} was kept constant for both fabrication steps. The final structure was developed in PGMEA and left to dry in air.

Epifluorescence Microscopy: Microstructures were analyzed in phosphate buffer saline (PBS) solution using an Olympus IX81 microscope equipped with a 60× objective, an Orca Flash camera, and a Lumencor Spectra X LED light source for the excitation of the photoinitiator, 7-Diethylamino-3-thenoylcoumarin. Microstructures were visualized under bright field and DAPI (4′-6-diamidino-2-phenylindole) excitation.

Confocal Microscopy: Confocal imaging was carried out using a Leica SP8 scanning confocal microscope equipped with a 20× objective and 3PMT detectors. Excitation wavelength chosen was ~488 nm using a pulsed White Light Laser. Microstructures contained the fluorescent photoinitiator, 7-Diethylamino-3-thenoylcoumarin to enable analysis.

Scanning Electron Microscopy (SEM): Scanning electron microscopy images of the microstructures were carried out on a Zeiss ULTRA plus microscope with a GEMINI FESEM column (Zeiss, Germany) operating at 2–5 kV under SE2 mode. An Au-Pd nano-scale thin layer (~10 nm) was coated on the microstructures as a conductive layer under argon atmosphere by coater (Cressington sputter coater 208HR). The Ag-Pd target (57 × 0.1 mm) for the coater was purchased from Ted Pella Inc. To obtain images of the microstructures in the hydrated state, a drop of deionized water was placed over the slides before freeze drying.

Atomic Force Microscopy (AFM): A commercial SPM system (MFP-3D, Asylum Research, USA) was used for measuring the swelling and mechanical properties of the micro-fabricated 3D structures. Imaging both in air and liquid medium (30 µL droplet of PBS or 5 mM fructose solution) was performed in contact mode, and height and deflection images were recorded. Data were recorded with 256 lines per scan direction and with a scan rate of 0.4 Hz and scan angle of 90°. AFM probe (Electrical all-in-one, BudgetSensors, Bulgaria) with 4 different platinum coated AFM cantilevers on a single AFM holder chip in which cantilever B with tip radius <25 nm, resonant frequency of ~80 Hz, and a spring constant of 2.7 N m^{-1} was used for topography and modulus measurements. The AFM height images were processed using Gwyddion AFM software (version 2.6), all images were 1st order plane fit flattened. Line profile data were obtained following image postprocessing and plotted using Igor pro-6.38. Young's modulus measurements were done in contact mode using force spectroscopy technique in Asylum software. Before carrying out force curves on the sample, the probe was calibrated to obtain the spring constant and deflection InvOLS (inverse optical lever sensitivity). The modulus values were obtained by fitting the extension part of the force curve with Hertz model. Force measurements were done in two different locations over the micro-cubes with a force distance of 3 µm, 3 force curves were collected at each point and the overall modulus value was reported by averaging 6 different forces curves over a single cube fabricated at a specific laser power.

Sugar-Induced Swelling and Actuation: For sugar-response analysis, an open cell-type arrangement was used. To hydrate the structures, a drop of PBS was added to top of the slide in a region marked by a hydrophobic pen. For sugar actuation, a drop of fructose solution (0.05, 0.1, 0.5, 1, 2.5, 5, 10, 15, 20, 25, and 100 mM in PBS) or of glucose solution (1, 10, 25, 50, 75, 100, 150, 200, 300, and 400 mM in PBS) was added to the marked region. A dust-free wipe was used to dry off excess solution. Area measurements were conducted using ImageJ from the microscopy images taken in each state.

FEA Simulation: Ansys workbench 2021 R1 was used to simulate the swelling of bilayer structures. The materials were considered as isotropic with no interfacial differences at the joints between layers or between the materials of the bilayer. The simulation also assumed complete permeation of the swelling such that the expansion was homogenous in the material. The simulation consisted of a two-step process to mimic the Dry⇒PBS⇒Fructose response. The material properties were calculated using the experimental cycling of PBA-based hydrogel pillars over 5 cycles (see Figure 2D) to calculate the swelling coefficients for each step. The geometric input for the PBS response simulation was the .stl file used to produce the beam samples, the geometry was meshed with 1.6 µm elements. The geometric output of the PBS response simulation provided the input geometry for the fructose response simulation for final geometry.

3D Design: Several of the 3D structures used in this work were designed using blender and DeScribe software and subsequently fabricated using the Photonic Professional GT system (Nanoscribe GmbH). The arrays of 4 × 4 cylindrical pillars (30 µm in height, 20 µm in diameter) were fabricated using a laser power range from 20 to 40 mW; scan speed 10 mm s^{-1}; slicing distance 0.3 µm; hatching distance 0.3; no contours. Bilayer structures were designed using MatLab codes created by Luke Dowling. The twisted vase structure was adapted from files licensed under the Creative Commons- Attribution 4.0 International (CC BY 4.0) license and available for download. Twisted vase structure by TK3DPrinting https://www.thingiverse.com/thing:2267093.

Supporting Information

Supporting Information is available from the Wiley Online Library or from the author.

Acknowledgements

A.E. and D.N. contributed equally to this work. This research received funding from the European Research Council (ERC) Starting grant (no. 802929 – ChemLife), Science Foundation Ireland (SFI), and European Regional Development Fund (ERDF) under grant number 12/RC/2278_P2. C.D. acknowledges support from the Irish Research Council through the Government of Ireland Postdoctoral Fellowship Scheme; grant number GOIPD/2020/484. L.F. and S.K. also acknowledge funding from the European Horizon 2020 Research and Innovation Programme (no. 899349 – 5D NanoPrinting). A.E. acknowledges Science Foundation Ireland (SFI) support under the SFI-AMBER PhD Recruitment scheme. Y.T. acknowledges SFI 18/EPSRC-CDT-3581 and the Engineering and Physical Sciences Research Council EP/S023259/1. A.J.T. was supported by the NIHR Imperial Biomedical Research Centre (BRC). The direct laser writing and the imaging for this project were carried out at the Additive Research Laboratory (AR-Lab) and the Advanced Microscopy Laboratory (AML), Trinity College Dublin, Ireland. The AR-Lab and AML are SFI supported centers, part of the CRANN Institute and affiliated to the AMBER center.

Open access funding provided by IReL.

Conflict of Interest

The authors declare no conflict of interest.

Data Availability Statement

The data that support the findings of this study are available in the supplementary material of this article.

Keywords

4D printing, boronic acid, microstructures, responsive structures, sugar responsive

Received: November 29, 2022
Revised: January 25, 2023
Published online:

[1] a) G. Ying, N. Jiang, C. Yu, Y. S. Zhang, *Bio-Des. Manuf.* **2018**, *1*, 215; b) E. M. Sánchez, J. C. Gómez-Blanco, E. L. Nieto, J. G. Casado, A. Macías-García, M. A. D. Díez, J. P. Carrasco-Amador, D. T. Martín, F. M. Sánchez-Margallo, J. B. Pagador, *Front. Bioeng. Biotechnol.* **2020**, *8*, 776.

[2] a) A. S. Gladman, E. A. Matsumoto, R. G. Nuzzo, L. Mahadevan, J. A. Lewis, *Nat. Mater.* **2016**, *15*, 413; b) H. Li, C. Tan, L. Li, *Mater. Des.* **2018**, *159*, 20.

[3] a) M. J. Villangca, D. Palima, A. R. Banas, J. Glückstad, *Light: Sci. Appl.* **2016**, *5*, 16148; b) Y. Lee, W. J. Song, J. Y. Sun, *Mater. Today Phys.* **2020**, *15*, 100258.

[4] X. Liu, J. Liu, S. Lin, X. Zhao, *Mater. Today* **2020**, *36*, 102.

[5] S. V. Walter, F. Ennen-Roth, D. Büning, D. Denizer, M. Ulbricht, *ACS Appl. Bio Mater.* **2019**, *2*, 2464.

[6] J. C. Breger, C. Yoon, R. Xiao, H. R. Kwag, M. O. Wang, J. P. Fisher, T. D. Nguyen, D. H. Gracias, *ACS Appl. Mater. Interfaces* **2015**, *7*, 3398.

[7] D. Jin, Q. Chen, T.-Y. Huang, J. Huang, L. Zhang, H. Duan, *Mater. Today* **2020**, *32*, 19.

[8] a) M. Dautta, M. Alshetaiwi, J. Escobar, P. Tseng, *Biosens. Bioelectron.* **2020**, *151*, 112004; b) S. Xu, A. C. Sedgwick, S. A. Elfeky, W. Chen, A. S. Jones, G. T. Williams, A. T. A. Jenkins, S. D. Bull, J. S. Fossey, T. D. James, *Front. Chem. Sci. Eng.* **2020**, *14*, 112; c) C. Zhang, M. D. Losego, P. V. Braun, *Chem. Mater.* **2013**, *25*, 3239.

[9] a) D. Roy, J. N. Cambre, B. S. Sumerlin, *Prog. Polym. Sci.* **2010**, *35*, 278; b) T. D. James, in *Creative Chemical Sensor Systems*, Springer, Berlin, Heidelberg **2007**, p. 107.

[10] a) Y. Liu, Y. Zhang, Y. Guan, *Chem. Commun.* **2009**, *14*, 1867; b) S. Xing, Y. Guan, Y. Zhang, *Macromolecules* **2011**, *44*, 4479.

[11] Z. Tang, Y. Guan, Y. Zhang, *Polym. Chem.* **2014**, *5*, 1782.

[12] C. Wang, B. Lin, H. Zhu, F. Bi, S. Xiao, L. Wang, G. Gai, L. Zhao, *Molecules* **2019**, *24*, 1420.

[13] a) Q. Dou, D. Hu, H. Gao, Y. Zhang, A. K. Yetisen, H. Butt, J. Wang, G. Nie, Q. Dai, *RSC Adv.* **2017**, *7*, 41384; b) M. Elsherif, M. U. Hassan, A. K. Yetisen, H. Butt, *ACS Nano* **2018**, *12*, 2283; c) A. Matsumoto, T. Kurata, D. Shiino, K. Kataoka, *Macromolecules* **2004**, *37*, 1502.

[14] M. Shibayama, T. Tanaka, in *Responsive Gels: Volume Transitions I*, Springer, Berlin, Heidelberg **1993**

[15] a) D. Gong, J. Cai, N. Celi, L. Feng, Y. Jiang, D. Zhang, *J. Magn. Magn. Mater.* **2018**, *468*, 148; b) D. Kim, Z. Hao, T. H. Wang, A. Ansari, presented at *2020 Int. Conf. on Manipulation, Automation and Robotics at Small Scales (MARSS)*, IEEE, Toronto, Canada **2020**; c) S. Lee, S. Kim, S. Kim, J.-Y. Kim, C. Moon, B. J. Nelson, H. Choi, *Adv. Healthcare Mater.* **2018**, *7*, 1700985; d) S. Lee, J.-Y. Kim, J. Kim, A. K. Hoshiar, J. Park, S. Lee, J. Kim, S. Pané, B. J. Nelson, H. Choi, *Adv. Healthcare Mater.* **2020**, *9*, 1901697.

[16] a) H. C. Sun, P. Liao, T. Wei, L. Zhang, D. Sun, *Micromachines* **2020**, *11*, 404; b) H. Ceylan, I. C. Yasa, O. Yasa, A. F. Tabak, J. Giltinan, M. Sitti, *ACS Nano* **2019**, *13*, 3353; c) C. Peters, O. Ergeneman, P. D. W. García, M. Müller, S. Pané, B. J. Nelson, C. Hierold, *Adv. Funct. Mater.* **2014**, *24*, 5269; d) O. Tricinci, D. De Pasquale, A. Marino, M. Battaglini, C. Pucci, G. Ciofani, *Adv. Mater. Technol.* **2020**, *5*, 2000540; e) H. Ceylan, N. O. Dogan, I. C. Yasa, M. N. Musaoglu, Z. U. Kulali, M. Sitti, *Sci. Adv.* **2021**, *7*, eabh0273.

[17] a) H. Zeng, P. Wasylczyk, G. Cerretti, D. Martella, C. Parmeggiani, D. S. Wiersma, *Appl. Phys. Lett.* **2015**, *106*, 111902; b) M. Zhang, H. Shahsavan, Y. Guo, A. Pena-Francesch, Y. Zhang, M. Sitti, *Adv. Mater.* **2021**, *33*, 2008605; c) M. del Pozo, C. Delaney, M. Pilz da Cunha, M. G. Debije, L. Florea, A. P. H. J. Schenning, *Small Structures* **2022**, *3*, 2100158.

[18] a) H. Zeng, D. Martella, P. Wasylczyk, G. Cerretti, J.-C. G. Lavocat, C.-H. Ho, C. Parmeggiani, D. S. Wiersma, *Adv. Mater.* **2014**, *26*, 2319; b) D. Martella, D. Antonioli, S. Nocentini, D. S. Wiersma, G. Galli, M. Laus, C. Parmeggiani, *RSC Adv.* **2017**, *7*, 19940; c) E. Descrovi, F. Pirani, V. P. Rajamanickam, S. Licheri, C. Liberale, *J. Mater. Chem. C* **2018**, *6*, 10428; d) D. Martella, S. Nocentini, D. Nuzhdin, C. Parmeggiani, D. S. Wiersma, *Adv. Mater.* **2017**, *29*, 1704047.

[19] a) M. Hippler, E. Blasco, J. Qu, M. Tanaka, C. Barner-Kowollik, M. Wegener, M. Bastmeyer, *Nat. Commun.* **2019**, *10*, 232; b) A. Tudor, C. Delaney, H. Zhang, A. J. Thompson, V. F. Curto, G.-Z. Yang, M. J. Higgins, D. Diamond, L. Florea, *Mater. Today* **2018**, *21*, 807; c) T. Spratte, S. Geiger, F. Colombo, A. Mishra, M. Taale, L.-Y. Hsu, E. Blasco, C. Selhuber-Unkel, *Adv. Mater. Technol.* **2023**, *8*, 2200714; d) Y. Liu, R. Liu, J. Qiu, S. Wang, *J. Adv. Manufact. Process.* **2021**, *4*, e10107.

[20] a) S. Rekštytė, D. Paipulas, M. Malinauskas, V. Mizeikis, *Nanotechnology* **2017**, *28*, 124001; b) C. Lv, X.-C. Sun, H. Xia, Y.-H. Yu, G. Wang, X.-W. Cao, S.-X. Li, Y.-S. Wang, Q.-D. Chen, Y.-D. Yu, H.-B. Sun, *Sens. Actuators, B* **2018**, *259*, 736; c) Y.-L. Zhang, Y. Tian, H. Wang, Z.-C. Ma, D.-D. Han, L.-G. Niu, Q.-D. Chen, H.-B. Sun, *ACS Nano* **2019**, *13*, 4041; d) Z. Xiong, M.-L. Zheng, X.-Z. Dong, W.-Q. Chen, F. Jin, Z.-S. Zhao, X.-M. Duan, *Soft Matter* **2011**, *7*, 10353.

[21] a) Q. Chen, P. Lv, T.-Y. Huang, J. Huang, H. Duan, *Adv. Intel. Syst.* **2020**, *2*, 1900128; b) J.-Y. Wang, F. Jin, X.-Z. Dong, J. Liu, M.-L. Zheng, *Adv. Mater. Technol.* **2022**, *7*, 2200276; c) Y. Hu, Z. Wang, D. Jin, C. Zhang, R. Sun, Z. Li, K. Hu, J. Ni, Z. Cai, D. Pan, X. Wang, W. Zhu, J. Li, D. Wu, L. Zhang, J. Chu, *Adv. Funct. Mater.* **2020**, *30*, 1907377; d) S. Wei, J. Liu, Y. Zhao, T. Zhang, M. Zheng, F. Jin, X. Dong, J. Xing, X. Duan, *ACS Appl. Mater. Interfaces* **2017**, *9*, 42247; e) R. Li, D. Jin, D. Pan, S. Ji, C. Xin, G. Liu, S. Fan, H. Wu, J. Li, Y. Hu, D. Wu, L. Zhang, J. Chu, *ACS Nano* **2020**, *14*, 5233; f) Z.-C. Ma, Y.-L. Zhang, B. Han, X.-Y. Hu, C.-H. Li, Q.-D. Chen, H.-B. Sun, *Nat. Commun.* **2020**, *11*, 4536; g) T. Y. Huang, H. W. Huang, D. D. Jin, Q. Y. Chen, J. Y. Huang, L. Zhang, H. L. Duan, *Sci. Adv.* **2020**, *6*, eaav8219.

[22] K. Kobayashi, C. Yoon, S. H. Oh, J. V. Pagaduan, D. H. Gracias, *ACS Appl. Mater. Interfaces* **2019**, *11*, 151.

[23] C. L. Lay, C. S. L. Koh, Y. H. Lee, G. C. Phan-Quang, H. Y. F. Sim, S. X. Leong, X. Han, I. Y. Phang, X. Y. Ling, *ACS Appl. Mater. Interfaces* **2020**, *12*, 10061.

[24] S. Harrisson, S. R. Mackenzie, D. M. Haddleton, *Macromolecules* **2003**, *36*, 5072.

[25] a) T. Elshaarani, H. Yu, L. Wang, J. Feng, C. Li, W. Zhou, A. Khan, M. Usman, B. U. Amin, R. Khan, *Int. J. Biol. Macromol.* **2020**, *161*, 109; b) O. B. Ayyub, M. B. Ibrahim, R. M. Briber, P. Kofinas, *Biosens. Bioelectron.* **2013**, *46*, 124; c) D. Bruen, C. Delaney, D. Diamond, L. Florea, *ACS Appl. Mater. Interfaces* **2018**, *10*, 38431.

[26] X. Wu, Z. Li, X.-X. Chen, J. S. Fossey, T. D. James, Y.-B. Jiang, *Chem. Soc. Rev.* **2013**, *42*, 8032.

[27] S. J. Angyal, R. S. Tipson, D. Horton, *Acad. Press* **1984**, *42*, 15.

[28] S. J. Angyal, D. Horton, *Acad. Press* **1991**, *49*, 19.